



Mechanisms and nonlinear damping behavior of innovative CFP-STF isolator

Li Sun · Tianqi Liang · Chunwei Zhang

Received: 2 January 2024 / Accepted: 20 June 2024 / Published online: 2 August 2024
© The Author(s), under exclusive licence to Springer Nature B.V. 2024

Abstract In recent years, the increasing demand for vibration control has driven the development of viscous damping isolators, and there have been many attempts to apply the shear thickening fluid (STF) system to vibration control to achieve customized damping property according to different application requirements. Previous studies on the performance of STF-based isolators have observed a peculiar “collapse” phenomenon, but researchers have no clear explanation for the mechanism causing this unfavorable phenomenon. The main focus of this work is to explore the nonlinear characteristics and mechanism of STF-based isolators, especially for introducing a novel carbon fiber powder STF system (CFP-STF). The damping mechanism of the CFP-STF isolator is theoretically derived based on Poiseuille’s law, the governing equations of arbitrary rheology are solved and demonstrated in details, and the theoretical model is established for multi-scale analysis under multi-frequency loading. To explore the influence of each parameter on the damping coefficient/force–displacement–velocity relationship, attention is paid to the

initial viscosity and peak viscosity of the CFP-STF system, and as a result the concept of damping coefficient decrease rate is proposed in this paper. The results show that the the new CFP-STF isolator avoids the “collapse” phenomenon of the force–displacement hysteresis curve at high frequencies, where the damping force does not decrease and the mechanical dissipation tends to increase linearly after the threshold is exceeded, since the viscosity decreases more slowly than the velocity increases with increasing frequency.

Keywords Carbon fiber powder (CFP) · Shear thickening fluid (STF) · Nonlinear isolator · Poiseuille’s law · Nonlinear damping · Damping mechanism

1 Introduction

In the field of civil engineering, it is important to reduce or control the vibration response of building structures because structural vibrations caused by external loads such as earthquakes and winds can reduce the reliability of the structure or even lead to disasters. Structural vibration control can be broadly categorized into passive control [1–4], semi-active control [5], active control [6, 7] and hybrid control [8] according to whether energy input is required during

L. Sun (✉) · T. Liang
School of Civil Engineering, Shenyang Jianzhu
University, Shenyang, People’s Republic of China
e-mail: sunli2009@sjzu.edu.cn

C. Zhang
Multidisciplinary Center for Infrastructure Engineering,
Shenyang University of Technology, Shenyang, People’s
Republic of China

use or whether control forces can be actively provided. Where the passive control relies on material properties to absorb or dissipate energy and therefore does not require additional energy input and signal acquisition systems [9]. Passive control systems have the advantages of simple structure, stable performance and well-defined energy dissipation capability. Damping elements are one of the essential components in vibration isolation devices in the field of passive control. Normally damping property exhibits significant control effectiveness of the response of a structure at resonance by dissipating vibration energy.

Traditional damping materials are mainly dimethyl silicone oil [10], metal matrix composites [11, 12], rubber [13], and thermoplastic polymers [14]. Isolator damping using conventional damping materials has a linear behavior that decreases the transmissibility in the resonance region, but increases the transmissibility in some frequency regions. This is a common problem with vibration isolators using linear viscous damping. In particular, traditional linear damping devices cannot change their physical properties with the change of external stimulation (e.g., frequency of vibration, etc.), and it has poor environmental adaptability and tunability [15]. Therefore, adaptive materials have attracted considerable interest from researchers, typical adaptive materials include electro-rheological (ER) elastomers/fluids [16], magneto-rheological (MR) fluids [17, 18], and shape memory alloys (SMAs) [19].

The traditional passive vibration isolators transmit a constant excitation force, but the vibration response of the isolated structure is different under different frequency excitation forces. Yu et al. [15, 20] developed a semi-active damper with adaptive variable stiffness and proposed a new phenomenological model for the controller design of the shear mode rotational magneto-rheological damper, and the results showed that the control scheme could adapt the building structure to different levels of seismic excitation. Hao et al. [21] proposed an isolator with both high static stiffness and low dynamic stiffness, and the results showed that a reasonable arrangement of stiffness and damping can improve the vibration isolation performance. Cai et al. [22] designed a variable-stiffness metamaterial isolation system that combines folded beams with positive stiffness and buckled beams with negative stiffness to isolate vibration in a small frequency gap. Shang et al. [1] investigated the

damping performance of a novel variable friction pendulum bearing system under the action of near-fault ground shaking. They found that the velocity-dependent indices have the greatest influence on the top plate displacement and isolator deformation, while the acceleration is mainly affected by the acceleration-dependent indices. This also shows that it is necessary to introduce a velocity-dependent material based on the friction-based isolator.

The shear thickening fluid is a kind of non-Newtonian fluid whose viscosity increases dramatically with the increase of shear rate or applied stress [23–25]. With the real-time change of the external excitation, the nonlinear isolator based on the STF system can adjust its dynamic properties in real time, reduce or even eliminate the response of the structure due to external vibration, and show different energy dissipation capabilities in the face of different frequency excitations, which is a great advantage compared with the traditional passive vibration isolator. György et al. [26] proposed a damping resolution method for predicting a viscous damper filled with a non-Newtonian fluid, which approximates the STF flow as a laminar Poiseuille flow. This study greatly simplified the damping prediction process for the STF-based nonlinear damper by reformulating the governing equations based on the shear stress versus viscosity curve, which can be solved for arbitrary rheological behavior. Zhao et al. [27] conducted theoretical and experimental studies on the damping effect of the STF-based damper under different mounting directions, vibration frequencies and amplitudes. The results show that the STF-based damper exhibits variable nonlinear damping at different shear rates, and its output damping force increases significantly with increasing frequency and amplitude. It does not require external energy input and can realize adaptive damping for different vibration frequencies and amplitudes. However, the experimental phenomenon of “vertical collapse” is obvious, but this study does not further explain the reason for this phenomenon. Sun et al. [28] proposed a novel compounded STF system based on carbon fiber powder (CFP), which solved the modulus instability and shear thinning problems of conventional STFs, and the key rheological performance indexes of the CFP-STF system were ten times or even more than those of conventional STFs. Therefore, CFP-STFs were used for further analysis in this work. Meanwhile, in the experiments

of STF dampers, the phenomenon of “collapse” appears in the hysteresis curves of force and displacement at the origin [27, 29–34], but none of these studies explains or analyzes this phenomenon, so this work focuses on analyzing the reasons for this phenomenon.

In this work, we take advantage of the adaptive energy dissipation of the CFP-STF, illustrate the structural design and working mechanism of the isolator, and discuss in detail the effects of shear thinning at high shear rates. The rest of the research is organized as follows. In Sect. 2, the equations for the rheological behavior of the CFP-STF system are developed and the model can be used to design the rheological and geometrical parameters. A detailed explanation of the rheological properties of CFP-STF was used in a previous work by the authors, and the parametric analysis of the rheological behavior of CFP-STF is omitted in this work. In Sect. 3, the structural design and working mechanism of the smart STF isolator are presented and theoretically modeled for analysis. In Sect. 4, the parametric effects of the CFP-STF based isolator are discussed and several models are compared at different speeds and frequencies.

2 Rheological model of CFP-STF

The STF system used in this study was derived from the CFP-STF system proposed by Sun et al. [29]. The diameter of the carbon fiber powder used was 7 microns and the length was 20–40 microns. Hydrophilic fumed silica nanoparticles were prepared with a microscopic average particle size of 12 nm. Polyethylene glycol 200 (PEG200) is a neutral transparent liquid with stable properties at room temperature. Its hydroxyl value is 510–623 mgKOHg⁻¹. The rheological properties of the CFP-STF system were measured in the rheological performance tests at 25 °C using a parallel plate rheometer (MCR 301, Anton Paar Companies, Germany). The rheometer plate diameter was 10 mm and the gap was set to 1 mm. Currently, there is no generalized method for calculating the flow behavior of non-Newtonian fluids inside an isolator to directly predict velocity-force damping characteristics. Researchers have commonly used the method of comparing measured data with fitted data [26, 31, 35]. This method can be used to obtain a continuous rate-

viscosity model for theoretical analysis while satisfying the accuracy. In this work, only three parametric variables are involved. Initial and peak viscosities are constructed as fitting parameters, which makes the rheological model more concise and meaningful.

$$\mu(\dot{\gamma}) = \exp(a + \eta_0 \ln(\dot{\gamma})/\dot{\gamma} - 1.142(\eta_{\max}/\eta_0)b/(\dot{\gamma}^2)), \quad (1)$$

where $\dot{\gamma}$ is the shear rate and represents the velocity to gap ratio between two parallel plates, a, μ_0 and μ_{\max} are all parameters that can be obtained from the CFP-STF rheological tests. The parameters were fitted using the Levenberg–Marquardt method and a generalized global optimization method for the CFP-STF system with a CFP mass fraction of 8% and nano-silica from previous research [28]. The fitted parameters in Eq. (1) can be obtained as $a = 4.5477$, $b = 1.1417$, $\eta_0 = 15.9826$, $\eta_{\max} = 1380.2800$. As shown in Fig. 1, only 29 iterations are required to complete the fitting and meet the accuracy requirements, with a correlation coefficient R-squared of 0.9965. Obviously, the rheological model proposed in this work includes the rheological characteristics of pre-ST, shear thickening and shear thinning in three stages at the same time. Where η_{\max}/η_0 is the ratio of the peak viscosity to the initial viscosity of the CFP-STF system, which can also be used as an index of the shear thickening ability of the STF.

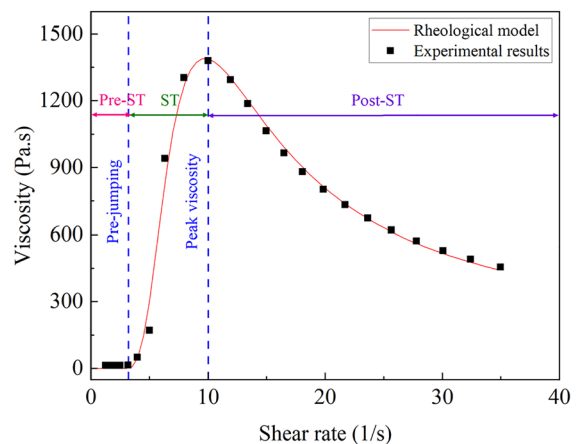


Fig. 1 Rheological property of CFP-STF system

3 Dynamic performance of the CFP-STF isolator

In this section, shear rate is used as a direct input to obtain the continuous viscosity profile of the CFP-STF system as shear rate increases. It will be more efficient to use the theoretical model presented in this work when the damping characteristics of an existing isolator need to be tailored to specific needs.

3.1 Conceptual design

This subsection describes the physical characteristics of the CFP-STF isolator. The main purpose here is to evaluate the dynamic nonlinear performance of the CFP-STF isolator under external excitation, rather than to discuss the effect of the material on the environment (e.g., external temperature). As shown in Fig. 2, the CFP-STF isolator consists of two main parts, the upper part consists of two columns (blue parts in the figure) connected by the upper cover plate and the grating. The lower part (orange part in Fig. 2) is mainly a chamber filled with CFP-STF. While the superstructure is excited to move in the x -direction, the internal CFP-STF will flow through the grating to another chamber, and the limit displacement of the isolator is determined by the width of the remaining chamber. On the other hand, the ends of the grating are designed to be chamfered, mainly to prevent energy

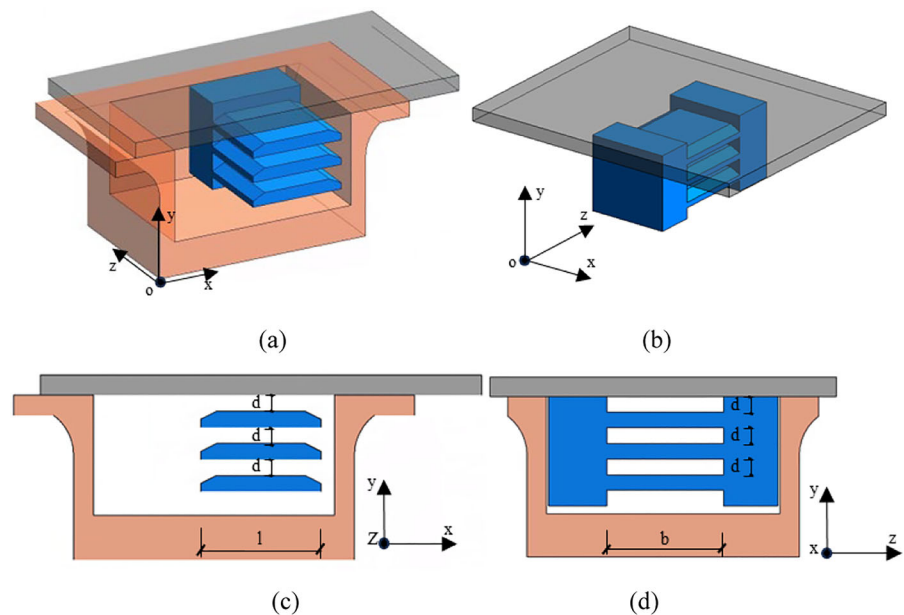
loss when the fluid flows through the edges of the grating.

3.2 Theoretical model

The dynamic performance of the CFP-STF isolator can be expressed by the equation $F = C(\dot{\mu})|\dot{\mu}|^\alpha \text{sgn}(\dot{\mu})$, where C is the damping coefficient of the isolator, F is the damping force provided by the isolator, α is the nonlinear coefficient, and $\dot{\mu}$ is the speed of motion of the grating. Therefore, the CFP-STF isolator has no stiffness and is only related to relative velocity. When the isolator is under sinusoidal excitation, the velocity is maximized when it passes through the displacement origin position. However, due to the velocity dependence in the damping term, the CFP-STF isolator is quite different from the traditional constant damping isolator.

As shown in Fig. 2, the length, width, and height of each grating gap of the CFP-STF are l , b , and d . Since the ST effect of the CFP-STF system is very obvious, the effect of the chamfered portion is neglected. The upper cover plate of the isolator moves along the x -direction at the same time as the CFP-STF system flows through the grating due to the pressure difference. Based on the theory of Poiseuille flow, the following assumptions can be presented: (1) the gap width d of CFP-STF in the grating is much smaller

Fig. 2 Detailed schematic construction of CFP-STF isolator



than l and b , and the fluid flow can be approximated by the pure Poiseuille flow between parallel plates; (2) CFP-STF is uniform and incompressible inside the grating, and it can be regarded as a one-dimensional problem; (3) the flow of CFP-STF belongs to the laminar flow; (4) the effect of acceleration can be neglected. It is known that the pressure difference varies linearly over the range of action of the CFP-STF system. The governing equation can be expressed in terms of the pressure gradient: $d\tau/dy = -\Delta P/L$, where τ is the shear stress and ΔP is the pressure difference. Figure 3 shows the profile distribution of shear velocity and shear stress of CFP-STF in the gap. Also, the continuity equation of the CFP-STF system can be expressed as $\tau = \mu(\dot{\gamma}) \frac{dv}{dy} = \mu(\dot{\gamma})\dot{\gamma}$, where v is the velocity of fluid motion in the grating gap, which is sinusoidally loaded in this work, and μ is the viscosity coefficient as a function of shear rate.

$$\frac{dv_{pr}}{dy} = -\frac{\Delta P}{L\mu_{pr}}y + A_1 \quad \dot{\lambda} \leq \dot{\lambda}_y, \tag{2}$$

$$\frac{dv_{st}}{dy} = -\frac{\Delta P}{L\mu_{st}}y + B_1 \quad \dot{\lambda} \geq \dot{\lambda}_y, \tag{3}$$

$$v_{pr} = -\frac{\Delta P}{2L\mu_{pr}}y^2 + A_1y + A_2 \quad \dot{\lambda} \leq \dot{\lambda}_y, \tag{4}$$

$$v_{st} = -\frac{\Delta P}{2L\mu_{st}}y^2 + B_1y + B_2 \quad \dot{\lambda} \geq \dot{\lambda}_y. \tag{5}$$

The rheological properties of the STF system, such as viscosity and shear modulus, increase rapidly when the shear rate exceeds the critical shear rate due to the “clustering” mechanism. The CFP-STF system used in this work has a more pronounced ST effect, with no

shear thinning behavior occurring prior to the ST effect. Therefore, the description of the relationship between shear stress and velocity in the CFP-STF isolator can be divided into two parts: before the occurrence of ST, as shown in Eq. (2), denoted by the subscript “pr”; and after the occurrence of ST, as shown in Eq. (3), denoted by the subscript “st”.

The undetermined constants A_1, A_2, B_1 and B_2 in the joint Eqs. (2–5) result from the integration of the governing equations. The boundary conditions for these coupled equations are mainly as follows: (1) the shear stress of the STF system at the edge of the grating gap is 0; (2) the rate of change of the flow velocity at the center point of the grating gap is 0, and the normal of the flow velocity curve at the center is perpendicular to the y -direction, as seen in Fig. 3; and (3) the grating motion speed is equal to the amount of change of the fluid flow velocity, i.e., $v(0) = v(d) = V(t)$, because the STF system is continuous and invariant in nature. The velocity Eq. (6) and flow Eq. (7) are obtained by solving the joint equations with boundary conditions and generalizing and simplifying:

$$v(y) = \frac{1}{2\mu(\dot{\gamma})} \frac{\Delta P}{L} (d - y^2) - V(t), \tag{6}$$

$$Q = b \int_0^d v(y)dy = b \int_0^d \left(\frac{1}{2\mu(\dot{\gamma})} \frac{\Delta P}{L} (d - y^2) - V(t) \right) dy. \tag{7}$$

In this work, the continuous function $\mu(\dot{\gamma})$ of the rheological behavior of the CFP-STF system is used, and the damping force and damping coefficient per unit time can be obtained from Eq. (8).

$$F_D = CV(t) = \Delta Pbd, \tag{8}$$

$$F = \frac{18L}{d^2} A_p V(t) \mu(\dot{\gamma}), \tag{9}$$

$$C = \frac{18L}{d^2} A_p \mu(\dot{\gamma}). \tag{10}$$

The theoretical model proposed in this work was compared with the isolator test results by substituting the rheological test results of the conventional STF system and the isolator parameters of Wei et al. [31] into Eq. (10), as shown in Fig. 4. The damping properties of the STF isolator vary at loading rates of 0.5 mm/s and 1 mm/s. The hysteresis curve collapses

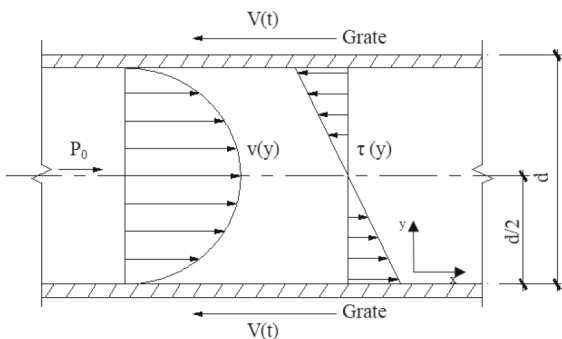


Fig. 3 Qualitative sketch of internal velocity and stress distribution in the grating gap

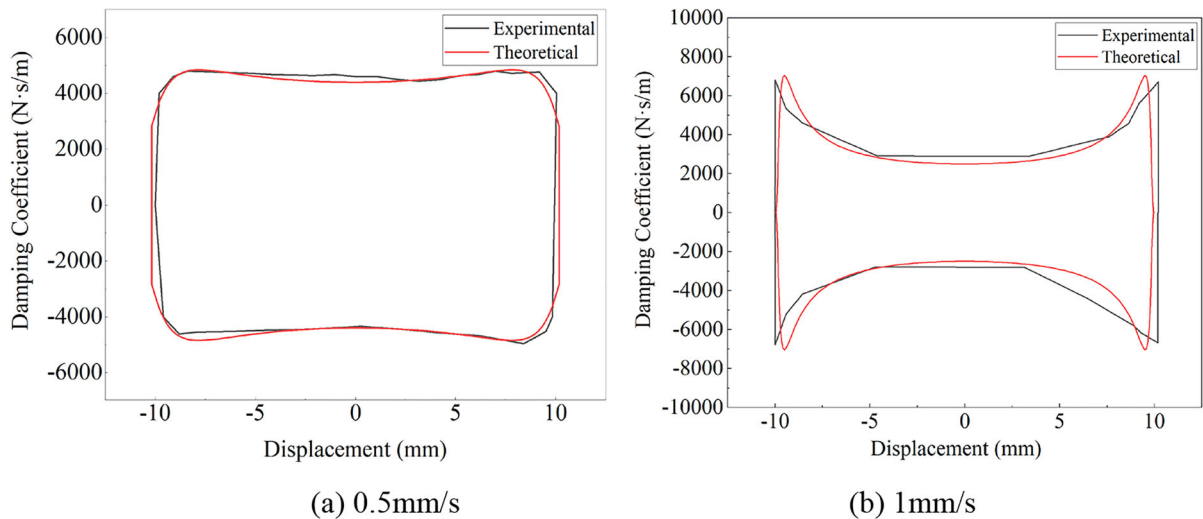


Fig. 4 Comparison of theoretical model and experimental results, **a**0.5 mm/s, **b**1 mm/s

when the loading rate exceeds a certain threshold. However, Wei et al. [31] did not provide an in-depth explanation of the mechanism behind this phenomenon. This paper presents a theoretical model that predicts the performance of the isolator accurately using a continuous rheological model, with a sharp increase and decrease in damping characteristics.

4 Results and discussions

This section examines the effect of frequency on the damping coefficient and damping force to investigate the nonlinear damping behaviors of the CFP-STF isolator. The sinusoidal excitation with a phase of 10 mm is used and the frequency range is set to 2–6 Hz with $b = 50$ mm, $l = 60$ mm and $h = 25$ mm, and the results are shown in Fig. 5.

The damping force and damping coefficient vary with frequency, as shown in Fig. 5a. Under the same conditions, the damping force increases nonlinearly with frequency and shows a rapid jump. At 2 Hz, the force–displacement hysteresis curve has a shuttle shape. This indicates weak energy dissipation capacity at this frequency. As the loading frequency increases, the curve becomes fuller and changes rapidly during 1–4 Hz, with the damping force increasing from 85.77 to 753.26 N (878%). After 4 Hz, the growth is slower, at only about 27 N (3%) per Hz.

The mechanism behind the phenomenon can be inferred from Fig. 6a, b. The CFP-STF system displays shear thickening between 0 and 4 Hz due to the “cluster” mechanism, and the force–displacement hysteresis curves demonstrate clear nonlinear behavior. The maximum viscosity of the CFP-STF system is reached at a frequency of 4 Hz. Beyond this frequency, the system enters the shear thinning phase. The loading mode is displacement-controlled sinusoidal loading. Therefore, the velocity of the CFP-STF system is maximum when passing through the displacement origin, and its shear velocity increases with the increase of frequency. As a result, the “collapse” phenomenon appears at the displacement origin in Fig. 5b. The damping force of STF starts to show linear behavior when the excitation frequency exceeds a certain threshold.

In this work, three new damping performance metrics, Point A and Point B, the key points in the hysteresis curve, and the rate of descent of the peak damping coefficient (ROD-DC) are proposed. Point A represents the “jumping point” where the shear thickening effect begins to appear in the dampening fluid, and point B represents the “sliding point” where the shear thickening behavior changes to the shear thinning stage. The initial viscosity η_0 of any STF system is relatively low, and in Fig. 6 it can be seen that both the force and damping coefficient at the displacement maximum are close to 0 (point A),

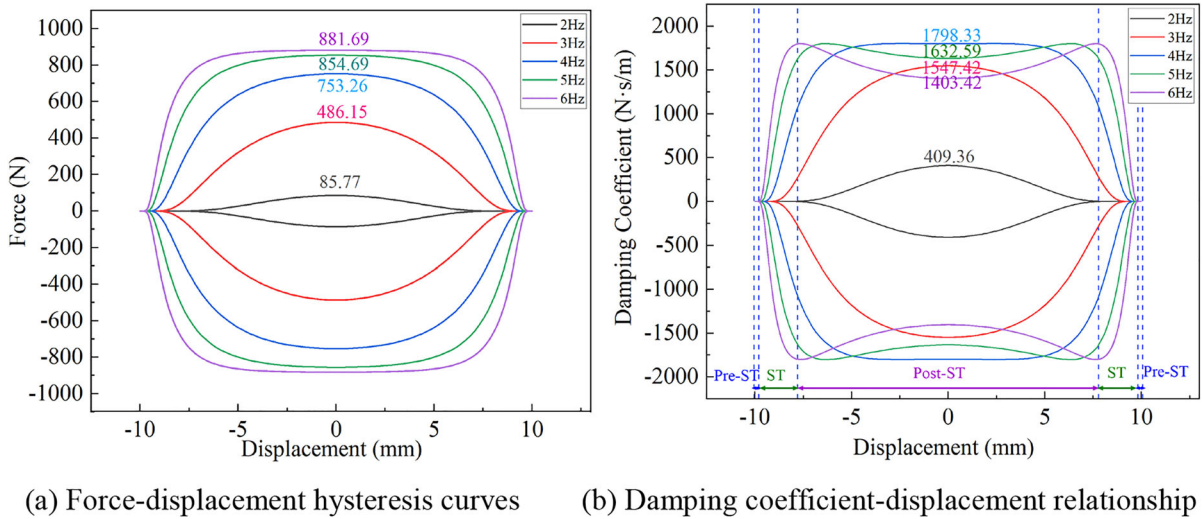


Fig. 5 Non-linear dynamic behaviors of the CFP-STF isolator under multi-frequency loading

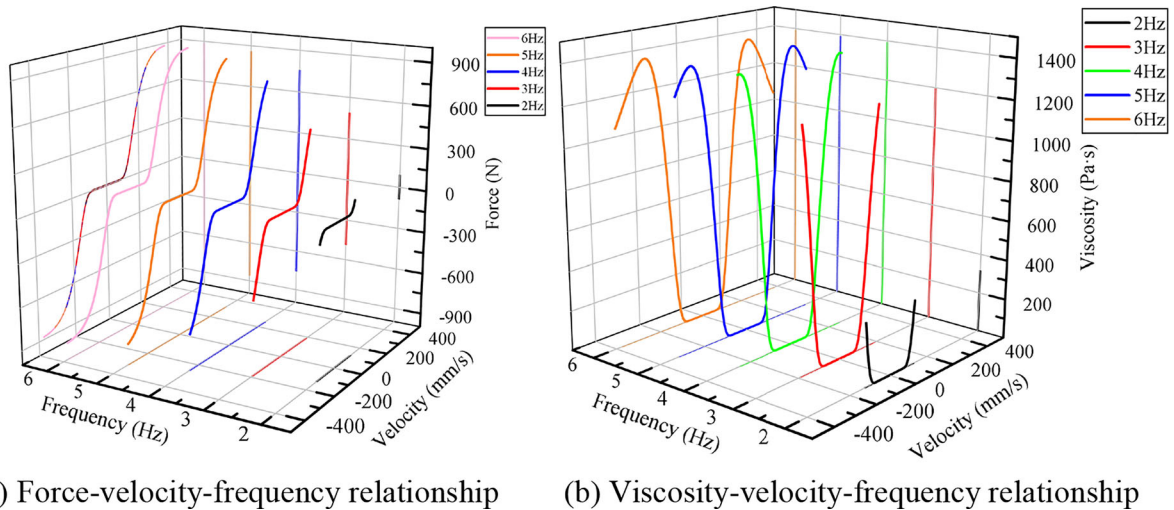
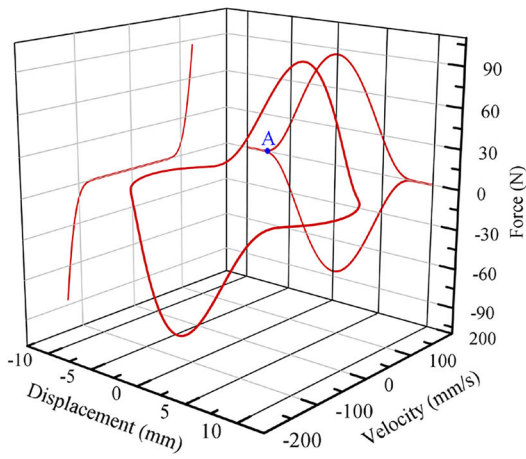


Fig. 6 Non-linear behaviors of force and viscosity under multi-frequency loading

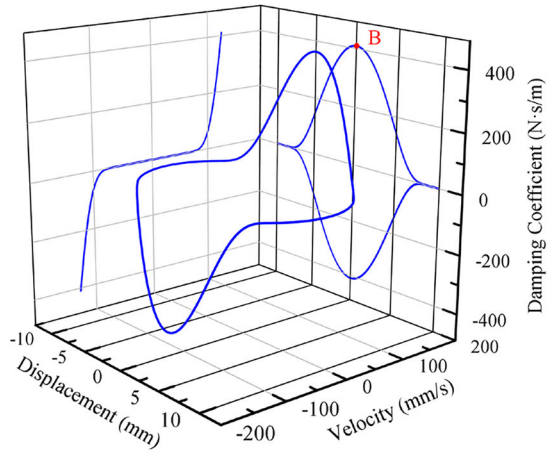
indicating that at the displacement maximum, i.e. when the velocity is close to 0, the damping fluid has not yet begun to exhibit shear thickening behavior. As the frequency is increased, the overall view of the hysteresis curve shows that the point A is moving further and further away from the origin of the displacement. The reason for this is that there is less time left for the shear thickening behavior if only the load frequency is increased.

As shown in Fig. 7, the vertical coordinate of point B represents the peak viscosity attenuation coefficient, which indicates the maximum damping that the CFP-

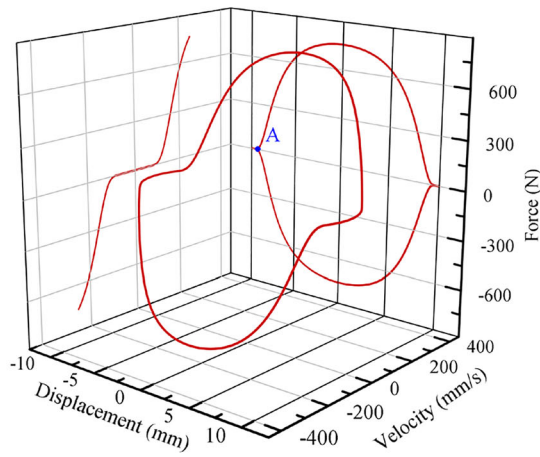
STF isolator can provide. As the loading frequency increases, point B begins moving away from the displacement origin, but the “collapse” phenomenon at the origin becomes more and more obvious. The metric ROD-DC is the ratio of the damping coefficients at the origin and those corresponding to point B, which is used to indicate the effect of shear thinning behavior. The damping coefficient increased by 439% (409.36 to 1798.33 N s/m) in the range of 1–4 Hz, and the damping coefficient corresponding to point B remained essentially unchanged after reaching 4 Hz. The lowest RODDC is 78% (1798.33 ~ 1403.42 N s/



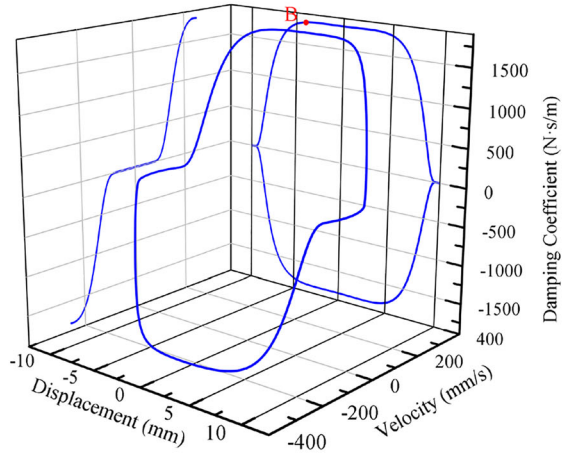
(a) 2Hz-Force



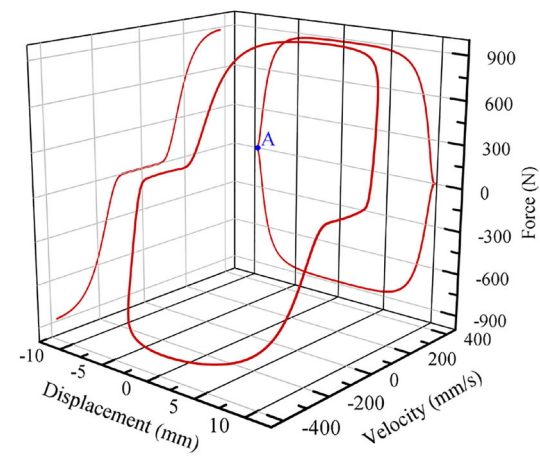
(b) 2Hz-Damping coefficient



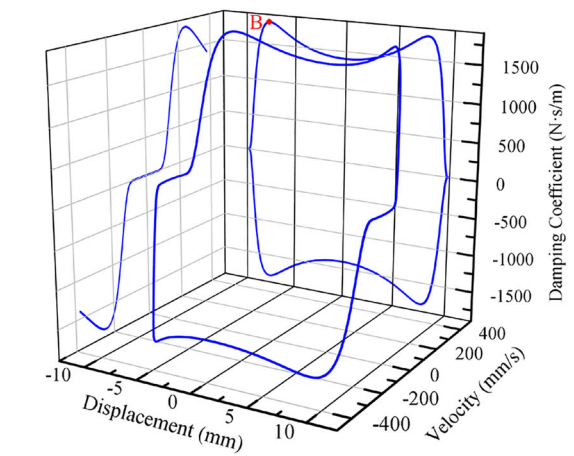
(c) 4Hz-Force



(d) 4Hz-Damping coefficient



(e) 6Hz-Force



(f) 6Hz-Damping coefficient

◀ Fig. 7 Displacement and Velocity Hysteresis Curve

m), indicating that the degree of collapse of the damping coefficient is related to the rate of viscosity decrease in the shear thinning stage of the STF system, which depends on its own rheological properties.

According to Eq. (8), the traditional fluid damper has a linear damping force that is proportional to the fluid viscosity. The relationship between damping force, mechanical energy consumption with damping coefficient and shear rate of the CFP-STF isolator is clearly shown in Fig. 8. Here, there is a very interesting phenomenon, the damping force reaches the threshold and then does not decrease but remains constant, the mechanical energy consumption always maintains a linear growth trend. The deeper reason is that after the CFP-STF reaches the shear rate threshold, the viscosity decreases more slowly than the shear rate increases. This also explains why the conventional STF system shows a force “collapse” phenomenon, while the CFP-STF system does not, because the rate of shear rate increase is not “complementary” to the rate of viscosity decrease. The CFP-STF system used in this work has a much better descent rate than the traditional STF system. This greatly improves the stability of the system while providing adaptive damping.

From the above analysis, the trend of STF isolator damping force, energy dissipation capacity and

working frequency range can be established under the situation of controllable output force, which can provide guidance for the design of working parameters in structural vibration control.

5 Conclusion

In this work, the dynamic nonlinear characteristics of a novel CFP-STF based isolator are investigated in detail. Multi-scale analysis is carried out for the variation of the damping coefficient/force–displacement-velocity of the CFP based isolator under the action of multi-frequency loading. The results show that the CFP-STF system exhibits faster response speed, and the damping force jumping behavior is obvious and rapid. Furthermore, the viscosity decreases slower than the velocity increases when the frequency increases, which avoids the phenomenon of force–displacement hysteresis curve “collapsing” at higher frequencies. As the loading frequency increases, the force–displacement hysteresis curve begins to become fuller, with the fastest rate of changing of the curve within 1–4 Hz, where the damping force increases rapidly from 85.77 to 753.26 N (878%), and grows slowly after 4 Hz, with an increase of only about 27 N (3%) per Hz. For the damping coefficient, the “collapse” phenomenon occurs with the increase of frequency, the peak damping coefficient remains basically unchanged

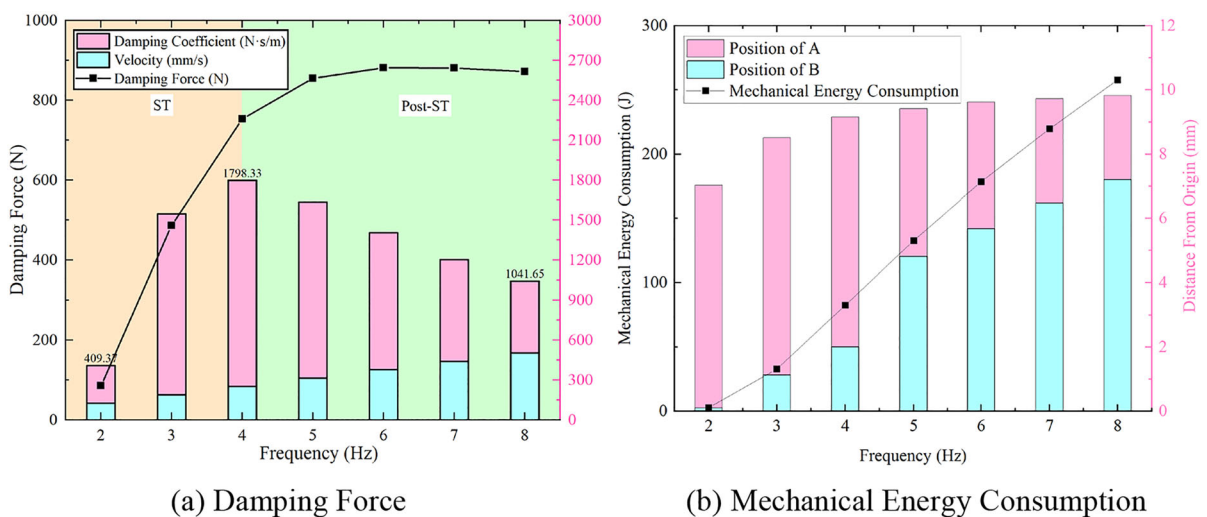


Fig. 8 Parametric effects of damping force and mechanical energy consumption

after reaching 4 Hz, and the higher the frequency, the more obvious the collapse at the origin of the displacement. 4–6 Hz frequency range of the ROD-DC is the lowest 78% (1798.33 ~ 1403.42 N·s/m). In this way, CFP-STF-based controlled structures can change their physical properties in response to changes in external excitations, acting as energy dissipative and damping materials in a wider region rather than as traditional damping materials limited to the resonance zone.

Acknowledgements The authors would like to thank the editors and reviewers for their valuable comments and suggestions.

Funding This research is financially supported by the National Natural Science Foundation of China (Grant Nos. 52378253, 52078310, and 52361135807), the Ministry of Science and Technology of China (Grant No. 2019YFE0112400), and the Department of Science and Technology of Shandong Province (Grant No. 2021CXGC011204).

Data availability Data will be made available on request.

Declarations

Conflict of interest The authors declare that they have no known competing financial interests or personal relationships that could have appeared to influence the work reported in this paper.

References

- Shang, J., Tan, P., Han, J., Zhang, Y., Li, Y.: Performance of seismically isolated buildings with variable friction pendulum bearings under near-fault ground motions. *J. Build. Eng.* **45**, 103584 (2022)
- Yi, J., Zhou, J.Y., Ye, X.J.: Seismic control of cable-stayed bridge using negative stiffness device and fluid viscous damper under near-field ground motions. *J. Earthq. Eng.* **26**(5), 2642–2659 (2022)
- Deringöl, A.H., Güneyisi, E.M.: Influence of nonlinear fluid viscous dampers in controlling the seismic response of the base-isolated buildings. *Structures* **34**, 1923–1941 (2021)
- Sun, L., Wang, G., Zhang, C., Sha, X.: Progress in shear thickening fluid study and its application in energy absorption and vibration reduction areas. *J. Shenyang Jianzhu Univ. (Nat. Sci.)* **39**(5), 1 (2023)
- Ohtori, Y., Christenson, R., Spencer, B., Dyke, S.: Benchmark control problems for seismically excited nonlinear buildings. *J. Eng. Mech.* **130**(4), 366–385 (2004)
- Spencer Jr, B.F., Christenson, R.E., Dyke, S.J.: Next generation benchmark control problem for seismically excited buildings, Kyoto Japan (1998)
- Afshar, D., Amin Afshar, M.: Nonlinear dynamic P-delta interaction between TMD and the frame structure under proportional internal resonances. *Struct. Control. Health Monit.* **29**(11), e3082 (2022)
- Wang, S.-J., Lee, B.-H., Chuang, W.-C., Chiu, I.C., Chang, K.-C.: Building mass damper design based on optimum dynamic response control approach. *Eng. Struct.* **187**, 85–100 (2019)
- Zhang, C., Ali, A.: The advancement of seismic isolation and energy dissipation mechanisms based on friction. *Soil Dyn. Earthq. Eng.* **146**, 106746 (2021)
- Kaleybar, R.S., Tehrani, P.: Effects of using different arrangements and types of viscous dampers on seismic performance of intermediate steel moment frames in comparison with different passive dampers. *Structures* **33**, 3382–3396 (2021)
- Siva Prasad, D., Shoba, C.: Damping behavior of metal matrix composites. *Trans. Indian Inst. Met.* **68**(2), 161–167 (2014)
- Mishra, S., Kumar, M., Kishor Sharma, Y.: Fabrication and characterization of nitinol reinforced metal matrix smart composite: a review. *Mater. Today Proc.* (2023). <https://doi.org/10.1016/j.matpr.2022.12.256>
- Zhao, J., Jiang, N., Zhang, D., He, B., Chen, X.: Study on optimization of damping performance and damping temperature range of silicone rubber by polyborosiloxane gel. *Polymers* **12**(5), 1196 (2020)
- Ali, A., Zhang, C., Bibi, T., Zhu, L., Cao, L., Li, C., Hsiao, P.C.: Investigation of five different low-cost locally available isolation layer materials used in sliding base isolation systems. *Soil Dyn. Earthq. Eng.* **154**, 107127 (2022)
- Yu, Y., Royel, S., Li, Y., Li, J., Yousefi, A.M., Gu, X., Li, S., Li, H.: Dynamic modelling and control of shear-mode rotational MR damper for mitigating hazard vibration of building structures. *Smart Mater. Struct.* **29**(11), 114006 (2020)
- Liu, W., Jin, H., Yao, J.: Vibration performance analysis of a self-energized damper composed of electrorheological fluid and piezoelectric ceramics. *Mech. Based Des. Struct. Mach.* **51**(10), 5968–5982 (2022)
- Zhang, G., Chen, J., Zhang, Z., Sun, M., Yu, Y., Wang, J., Cai, S.: A novel parametric model for nonlinear hysteretic behaviours with strain-stiffening of magnetorheological gel composite. *Compos. Struct.* **318**, 117082 (2023)
- Nie, S., Gong, F., Ji, H., Zhang, L., Ma, Z., Yin, F.: Effects of micron–nano composite iron particle powders on the tribological properties of magnetic fluids used for a nonlinear energy sink vibration absorber. *Phys. Fluids* **35**(9), 092012 (2023)
- Zhang, J.G., Ma, Z.H., Liu, F.F., Zhang, C.W., Sharafi, P., Rashidi, M.: Seismic performance and ice-induced vibration control of offshore platform structures based on the ISO-PFD-SMA brace system. *Adv. Mater. Sci. Eng.* **2017**, 1–15 (2017)
- Yu, Y., Hoshyar, A.N., Li, H., Zhang, G., Wang, W.: Nonlinear characterization of magnetorheological elastomer-based smart device for structural seismic mitigation. *Int. J. Smart Nano Mater.* **12**(4), 390–428 (2021)
- Hao, R.-B., Lu, Z.-Q., Ding, H., Chen, L.-Q.: A nonlinear vibration isolator supported on a flexible plate: analysis and experiment. *Nonlinear Dyn.* **108**(2), 941–958 (2022)
- Cai, C., Zhou, J., Wu, L., Wang, K., Xu, D., Ouyang, H.: Design and numerical validation of quasi-zero-stiffness

- metamaterials for very low-frequency band gaps. *Compos. Struct.* **236**, 111862 (2020)
23. Gürgen, S., Kuşhan, M.C., Li, W.: Shear thickening fluids in protective applications: a review. *Progress Polym. Sci.* **75**, 48–72 (2017)
 24. Sun, L., Wang, G., Zhang, C., Jin, Q., Song, Y.: On the rheological properties of multi-walled carbon nanopolyvinylpyrrolidone/silicon-based shear thickening fluid. *Nanotechnol. Rev.* **10**(1), 1339–1348 (2021)
 25. Zarei, M., Aalaie, J.: Application of shear thickening fluids in material development. *J. Mater. Res. Technol.* **9**(5), 10411–10433 (2020)
 26. Nagy-György, P., Hős, C.: Predicting the damping characteristics of vibration dampers employing generalized shear thickening fluids. *J. Sound Vib.* **506**, 116116 (2021)
 27. Zhao, Q., Yuan, J., Jiang, H., Yao, H., Wen, B.: Vibration control of a rotor system by shear thickening fluid dampers. *J. Sound Vib.* **494**, 115883 (2021)
 28. Sun, L., Liang, T., Zhang, C., Chen, J.: The rheological performance of shear-thickening fluids based on carbon fiber and silica nanocomposite. *Phys. Fluids* **35**(3), 032002 (2023)
 29. Urda, P., Pérez, J., Carabias, E., Cabrera, J.A., Castillo, J.J.: Design and testing of a steering damper for motorcycles based on a shear-thickening fluid. *Smart Mater. Struct.* **31**(9), 095031 (2022)
 30. Wei, M., Lin, K., Liu, H.: Experimental investigation on hysteretic behavior of a shear thickening fluid damper. *Struct. Control. Health Monit.* **26**(9), e2389 (2019)
 31. Wei, M., Lin, K., Guo, Q., Sun, H.: Characterization and performance analysis of a shear thickening fluid damper. *Meas. Control* **52**(1–2), 72–80 (2019)
 32. Zhou, H., Yan, L., Jiang, W., Xuan, S., Gong, X.: Shear thickening fluid-based energy-free damper: design and dynamic characteristics. *J. Intell. Mater. Syst. Struct.* **27**(2), 208–220 (2014)
 33. Yeh, F.-Y., Chang, K.-C., Chen, T.-W., Yu, C.-H.: The dynamic performance of a shear thickening fluid viscous damper. *J. Chin. Inst. Eng.* **37**(8), 983–994 (2014)
 34. Wei, M., Hu, G., Li, L., Liu, H.: Development and theoretically evaluation of an STF-SF isolator for seismic protection of structures. *Meccanica* **53**(4–5), 841–856 (2017)
 35. Lin, K., Wei, M., Qi, J.: Mechanical behavior of a torsional shear thickening fluid damper. *Smart Mater. Struct.* **32**(10), 105029 (2023)

Publisher's Note Springer Nature remains neutral with regard to jurisdictional claims in published maps and institutional affiliations.

Springer Nature or its licensor (e.g. a society or other partner) holds exclusive rights to this article under a publishing agreement with the author(s) or other rightsholder(s); author self-archiving of the accepted manuscript version of this article is solely governed by the terms of such publishing agreement and applicable law.